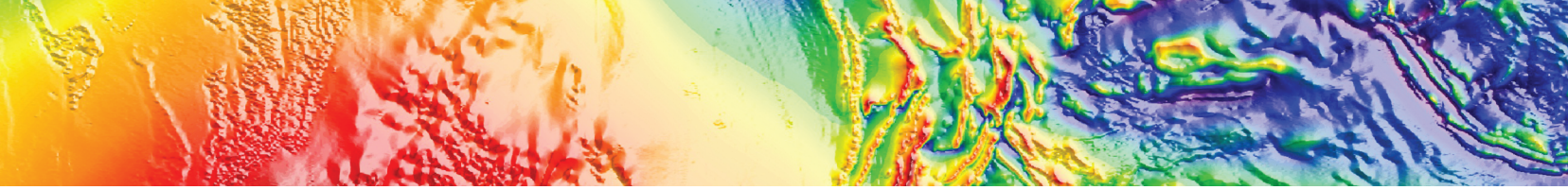

APPENDIX 6 SEISMIC REFRACTION METHOD

A6.1 Introduction

The *seismic refraction* method involves the analysis of the travel times of arrivals that travelled roughly parallel to the upper surface of a layer during their journey through the subsurface. These are direct arrivals (see Section 6.4.3.2) and critically refracted arrivals (see Section 6.3.4.2) as is implied by the method's name; although it is an unfortunate term, since refraction is a ubiquitous phenomenon affecting virtually every seismic arrival during its journey through the subsurface. For simplicity and consistency with common practice, these arrivals are referred to here as *refracted arrivals*, or just *refractions*.

Refraction surveys are only capable of mapping boundaries between zones where seismic waves travel at significantly different velocity. During interpretation it is usually assumed that the subsurface comprises a series of discrete layers within which the seismic velocity is constant or varies in a simple manner. It provides lower resolution of the subsurface than the reflection method, but the simpler acquisition and processing involved mean that the refraction method is much cheaper to apply. Common applications in the mining industry include:

- Determining the thickness of sedimentary cover overlying bedrock. This may be to determine the amount of cover material that needs to be stripped prior to mining (Goulty and Brabham, 1984) or the thickness of poorly consolidated materials as might be encountered in the kinds of geological environments where placer deposits occur (Lawton and Hochstein, 1993). The detection and delineation of palaeochannels is another exploration application (Pakiser and Black, 1957).
- Determining the thickness of the regolith in weathered terrains, provided the transition to unweathered material is not too gradual (Dentith *et al.*, 1992).
- Defining the basic form of the subsurface geology, usually by mapping some (velocity) marker horizon in the local stratigraphy.

The seismic refraction method has not been used in the mining industry as widely as other geophysical methods. Consequently, we provide here only a description of the fundamental aspects of the method. The reader requiring greater detail is referred to the descriptions given by Lankston (1990).

A6.2 Acquisition and processing of seismic refraction data

Refraction surveys use a linear spread, i.e. the detectors and the sources are all located along a single survey line (Fig. A6.1). The length of the spread, i.e. the distance between the shot and the most distant detector, needs to be about 10 times as long as the depth of investigation. Unambiguous interpretation of the data requires repeat recordings with the detectors in the same positions and the sources in different locations. Normal practice would be to have one or more sources within the line of detectors, plus end sources and one or more off-end sources at each end of the line. Continuous coverage of target layers is achieved by moving the entire spread and repeating the procedure.

Digital processing of the traces is minimal, usually comprising some form of frequency filtering (see Section 2.7.4). The most important processing step is determining the travel times of the various arrivals.

A6.2.1 Picking arrival times

Recall that a seismic trace is a representation of ground deformation versus time since the seismic source was

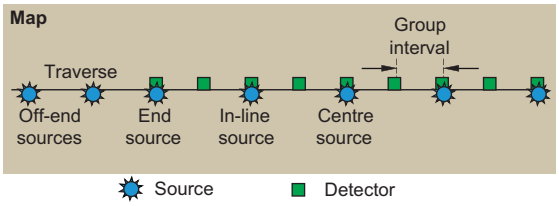

Figure A6.1 Schematic illustration of a spread used for 2D seismic refraction surveying.

activated, and the passing of a wavefront causes a deflection of the trace. The travel time of an arrival can be determined by identifying the point on the trace when the effects of the seismic wave first appear. This process is known as *picking* (with the result called a *pick*), and a wiggle trace is usually the best form of display to work with (see Fig. 6.12). Recognising the onset of an arrival involves identifying a change or '*break*' in the character of the trace from its pre-arrival state, in terms of amplitude, and/or frequency, and/or phase. The pick of the initial change in the trace from its undisturbed state is known as the *first break*. Identifying the first break is usually quite easy, but for later arrivals it requires careful observation of the form of the trace to identify what may be a subtle change in its character. There are a variety of computer algorithms available for picking arrivals in refraction data, with many of these using multiple criteria for identifying an arrival: see Hatherly (1982). Picking errors of 1 ms are typical for shallow refraction surveys.

Determining the onset time of later (non-first) arrivals is usually difficult because it is often obscured by the tail end of the earlier arrivals. Fortunately, the refracted arrivals used in the refraction method normally are the first to arrive at a given detector, and when multiple shots are recorded it is possible to infer the travel times of some of the later arrivals indirectly (see Section A6.3.2.4).

A6.3 Interpretation of seismic refraction data

Seismic refraction data are mostly interpreted using inverse methods (see Section 2.11.2.1). The input parameters to the inversions are the travel times of selected arrivals, and the locations of the detectors and the sources. For the most commonly used methods, it is necessary to group arrivals that have followed equivalent paths through the subsurface, which is usually done manually and may be time-consuming. Once this is achieved, the methods for inverting the travel time data are straightforward, but if the grouping of arrivals is incorrect the inversion will not produce the correct result.

A6.3.1 Travel times of critically refracted arrivals

Figure A6.2a shows a shot gather with well-defined first breaks. The first breaks define two roughly linear segments or branches. Figures A6.2b and c show a time–distance (T–X) graph and a raypath diagram for the simple case of a two-layer Earth. There is a planar and horizontal velocity interface between the layers: the upper layer has lower velocity (V_1) and the underlying layer a higher velocity (V_2). This velocity distribution allows critical refraction to occur (see *Critical refraction* in Section 6.3.4.2).

Arrivals at short offsets are direct arrivals, and their travel time (T) is given by:

$$T_{\text{direct}} = \frac{X}{V_1} \qquad \text{(A6.1)}$$

where X is the *offset*. This defines branch 1 of the T–X graph and it passes through the source location at zero

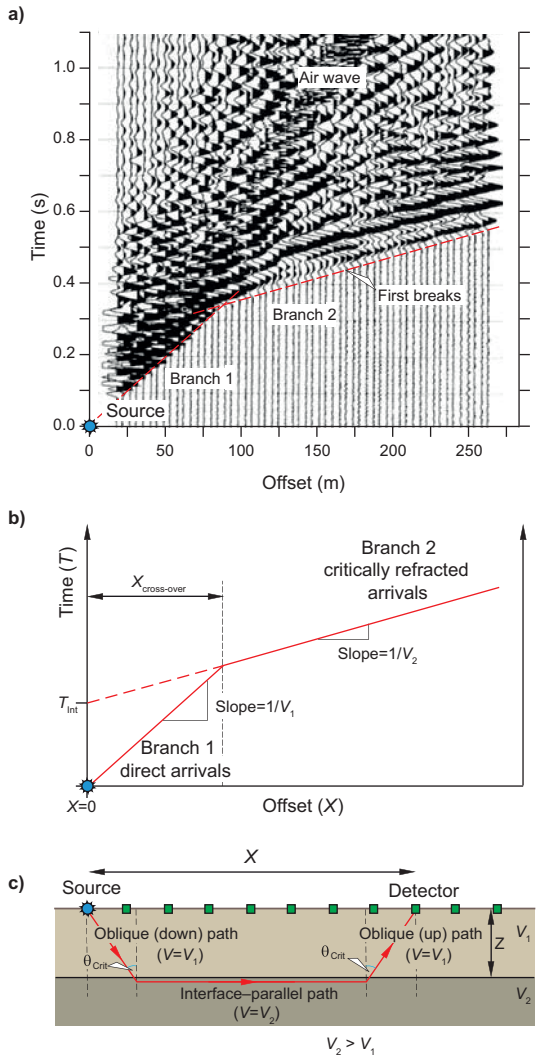

Figure A6.2 Time–distance data for critically refracted arrivals. (a) Shot gather showing two travel time branches defined by the change in slope of the first arrivals. Redrawn, with permission, from Miller *et al.* (1998). (b) Travel time graph for direct and critically refracted arrivals. (c) Raypaths showing critical refraction at a horizontal planar interface.

travel time. The reciprocal of its slope is the seismic velocity of the first layer, as described in Section 6.4.3.2. The expression for the travel times of critically refracted arrivals is:

$$T_{\text{Refr}} = T_{\text{source-B}} + T_{\text{B-C}} + T_{\text{C-detector}} = \frac{Z}{V_1 \cos\theta_{\text{Crit}}} + \frac{(X - 2Z\tan\theta_{\text{Crit}})}{V_2} + \frac{Z}{V_1 \cos\theta_{\text{Crit}}} \quad \text{(A6.2)}$$

where θ_{Crit} is the *critical angle* and Z is depth to the interface. This equation defines branch 2 of the T–X graph. Note that it does not extend to zero offset ($X = 0$) because of the oblique incidence associated with critical refraction.

The oblique segments of the paths are travelled at the lower velocity V_1, whilst the segment parallel to the interface is travelled at the higher velocity V_2. As the proportion of the raypath travelled at V_2 increases, the refracted waves eventually arrive before the direct arrivals. This occurs at offsets greater than $X_{\text{cross-over}}$ and is due to the direct waves following a more direct but lower-velocity path, so they are eventually overtaken.

Equation (A6.2) can be restated in terms of a constant component (T_{Int}, Fig. A6.2b) and a variable component describing the moveout as:

$$T_{\text{Refr}} = \frac{X}{V_2} + \frac{2Z\cos\theta_{\text{Crit}}}{V_1} \quad \text{(A6.3)}$$

At zero offset ($X = 0$) the expression becomes that for the intercept time:

$$T_{\text{Int}} = \frac{2Z\cos\theta_{\text{Crit}}}{V_1} \quad \text{(A6.4)}$$

The variable component (X/V_2) defines a straight line with slope $1/V_2$. The change in travel time with increasing offset (X) is solely due to travelling a greater distance, parallel to the interface, at the higher velocity V_2, and is not determined by the oblique parts of the raypaths whose lengths remain constant.

Clearly, by using the travel times of the arrivals, the velocities of the layers above and below the reflection interface can be determined from the slope of the direct and critically refracted arrivals on the T–X graph. The critical angle (θ_{Crit}) can then be determined from Eq. (6.14) (see Section 6.3.4.2).

Depth to the interface can then be obtained from the intercept time by rearranging Eq. (A6.4):

$$Z = \frac{T_{\text{Int}} V_1}{2\cos\theta_{\text{Crit}}} \quad \text{(A6.5)}$$

For completeness, we note that other forms of the travel time and intercept time equations are in common use, notably:

$$T_{\text{Refr}} = \frac{X}{V_2} + \frac{2Z\sqrt{V_2^2 - V_1^2}}{V_1 V_2} \quad \text{(A6.6)}$$

and

$$Z = \frac{T_{\text{Int}} V_1 V_2}{2\sqrt{V_2^2 - V_1^2}} \quad \text{(A6.7)}$$

Equivalent expressions exist for cases where there are more than two layers, the layers are dipping etc.; see for example Palmer (1986).

A6.3.2 Analysis of travel time data

Data from multiple spread and source positions are plotted in the same coordinate frame to create a group of T–X graphs. Note that unless otherwise stated, only first arrivals are plotted in the T–X graphs in the following description. This simplifies the explanation and corresponds with common practice, given the difficulty of directly identifying later arrivals.

Recognising individual branches and assigning them to a particular travel path (e.g. direct arrivals, refracted arrivals from the top of a particular layer etc.) requires simultaneous analysis of arrivals from different sources; without this the process is ambiguous, as is demonstrated by Ackermann *et al.* (1986). Data recorded with the sources located at opposite ends of the line of detectors are especially important since they provide *reversal* (data recorded with the seismic waves travelling in opposite directions along the line of detectors).

Figure A6.3 demonstrates the principles used to assign arrivals to branches using simple velocity models of the subsurface.

A6.3.2.1 Planar velocity layering

Figure A6.3a shows the T–X graph for a two-layer model, illustrating the most fundamental relationship between T–X graphs and velocity layering: that the number of layers is equal to the number of branches in the T–X graph. In practice there may be many identifiable branches, with branches at increasing offsets corresponding with arrivals from increasingly deeper layers.

For a horizontally layered Earth model (Fig. A6.3a), the T–X graphs produced from each of the three sources have the same shape and they can be overlaid after translation parallel to the location axis. Reflection in the horizontal

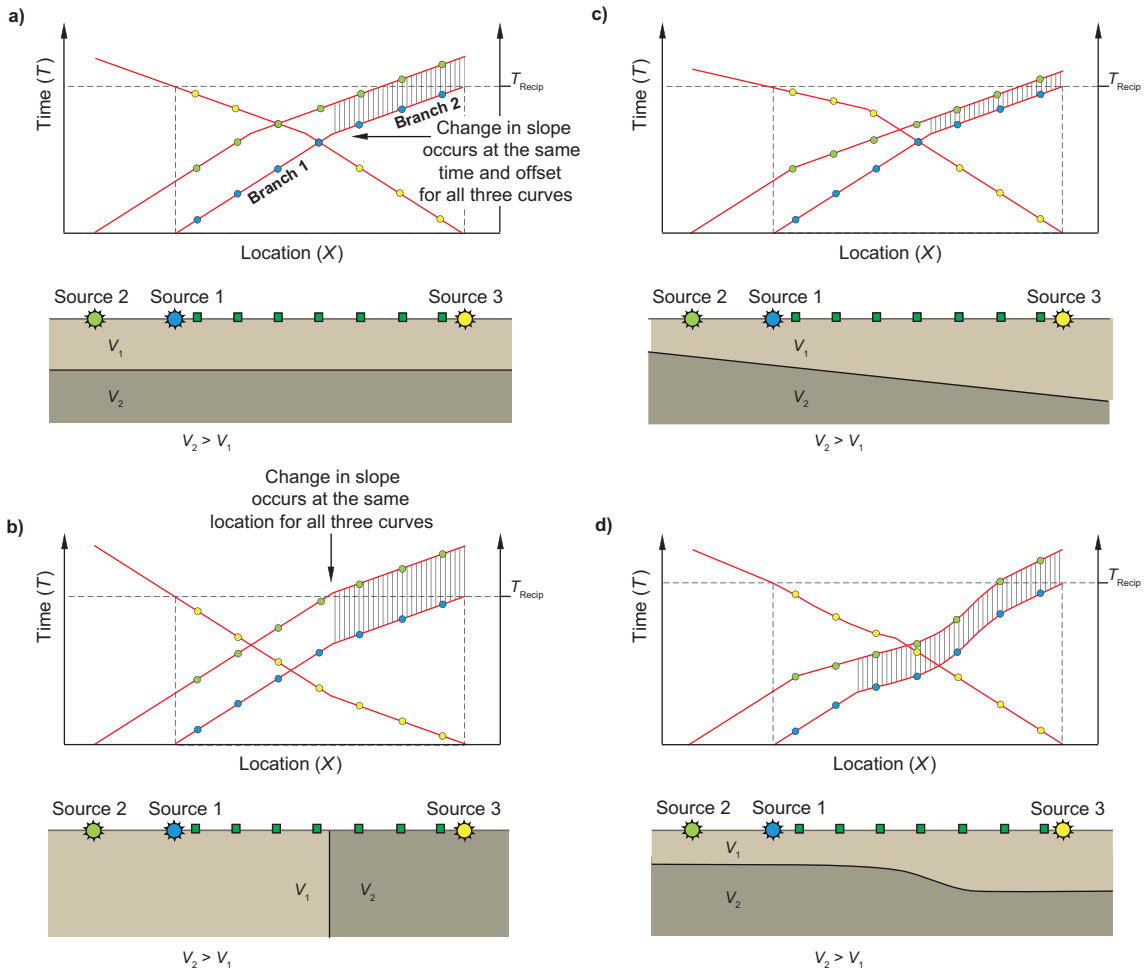

Figure A6.3 Time–distance (T–X) graphs produced by various subsurface velocity distributions. The vertical hatching indicates the locations where the T–X graphs for sources 1 and 2 are parallel. T_{Recip} – reciprocal time.

axis is also required for the graph recorded in the reverse direction (from source 3). This demonstrates that the transition from one branch to the next occurs at the same travel time and offset but, importantly, at different locations. Cross-over distances and intercept times are all the same.

The effects of lateral changes in velocity on T–X data are shown in Fig. A6.3b. As expected, two subsurface velocity layers produce two T–X branches, but the graphs for the individual sources are significantly different. Unlike the horizontal-layer case, the transition from one branch to the next occurs at the same locations and at different times and offsets. For this case, the various T–X graphs will coincide after a translation parallel to the time axis, with data recorded in the reverse direction (source 3) requiring reflection in the vertical axis.

Where a planar interface is dipping but does not intersect the surface within the spread, the shapes of the T–X graphs from each source are different again (Fig. A6.3c). Comparison of the data from the three sources shows that the deeper the interface below the source location, the greater are the intercept time and the cross-over distance. Furthermore, the slopes of the refracted-arrival branches are different depending on whether the line of detectors is located up-dip or down-dip from the source. Down-dip recordings have a steeper slope than up-dip recordings, and the reciprocals of the slopes do not represent the true velocity of the lower layer (V_2). The slope reciprocals instead are *apparent velocities*, being greater than the true velocity for up-dip recording and lower for down-dip recording. The difference in apparent velocities for reversed recordings indicates the dip direction of the interface. In the absence of reversed data it would not be possible to be sure that the interface was dipping; and if the interface was assumed to be horizontal, its depth and velocity determined using Eq. (A6.5) or (A6.7) would be erroneous.

A6.3.2.2 Non-planar velocity layering

The *T*–*X* graph resulting from constant velocity layers separated by an irregular interface is shown in Fig. A6.3d. The relief on the refracting interface means that the branches associated with refracted arrivals are no longer straight lines. Where the interface is deeper the travel times are greater, creating an approximate mirror image of the form of the interface itself in non-direct arrivals, albeit laterally displaced in the direction the waves are travelling. Note that a change in the dip of a planar interface can produce an abrupt reduction in the slope of the *T*–*X* graph, mimicking the effect of arrivals from an additional layer. Again, reversed data remove this ambiguity.

A6.3.2.3 Assigning arrivals to travel time branches

Based on the basic relationships between *T*–*X* data and velocity variations in the subsurface, the interpreter should be able to characterise each arrival (e.g. direct arrival etc.) according to the path taken from source to detector, and fit an internally consistent series of *T*–*X* branches to the data. In so doing, the basic form of the subsurface is defined, i.e. the number of layers and the general shape and orientation of interfaces separating the layers. During this process the arrival times of non-first arrivals, or even unrecorded refracted arrivals, can also be determined, the accuracy of individual picks assessed and the correctness of assigning data points to branches checked. These statements are, of course, subject to the caveat that the spacing of the shots and detectors is sufficiently small that the travel time variations in the survey area are correctly represented.

The data in Fig. A6.3 illustrate an important property of *T*–*X* graphs. Where refracted arrivals from the same interface are recorded in the same direction with different source locations, the travel time graphs may be superimposed by a vertical translation. This property is known as *parallelism* and is very useful for determining whether arrivals are from the same interface when assigning data to branches. If the branches are not parallel within measurement error, then the two arrivals at the relevant detectors did not come from the same layer.

The reversed data in Fig. A6.3 demonstrate another important property of *T*–*X* data: that the time to travel between two points is the same regardless of the direction of travel of the waves. For example, the travel time from source 1 to a detector at the location of source 2 is the same as that from source 2 to a detector at the location of source 1. These travel times are known as the *reciprocal time* (T_{Recip}) and the fact that they should be identical, within error, provides a useful check on the accuracy of a dataset.

A6.3.2.4 Phantoming

After the data points have been assigned to *T*–*X* branches using parallelism and reciprocal times, they can be consolidated into a subset comprising, for each layer, reversed refracted arrivals that extend across as much of the dataset as is possible. This is achieved using a technique known as *phantoming*, and the resultant subset contains all the information required for interpretation.

Phantoming is the extrapolation of the travel time branch defined by refracted arrivals, recorded from a source, to longer and/or shorter offsets. Most usually the *T*–*X* branch is extended back to zero-offset or beyond. Phantoming is only possible because of parallelism, as is demonstrated in Fig. A6.4. The time differences between corresponding points on two parallel segments are averaged to obtain the average time difference (ΔT) between the two *T*–*X* graphs (datasets). Phantoming simply involves adding, or subtracting where appropriate, ΔT from all the arrival times of one of the sources in order to superimpose the data onto those from another source. Ideally, the arrivals from the two sources will then coincide over their common location interval. Errors in ΔT propagate to all the data points, so results will be more reliable when the two datasets have a large number of overlapping points from which can be obtained a better estimate of ΔT. From the coincidence of the graphs, missing points such as those from source 1 in Fig. A6.4 can be obtained; but more

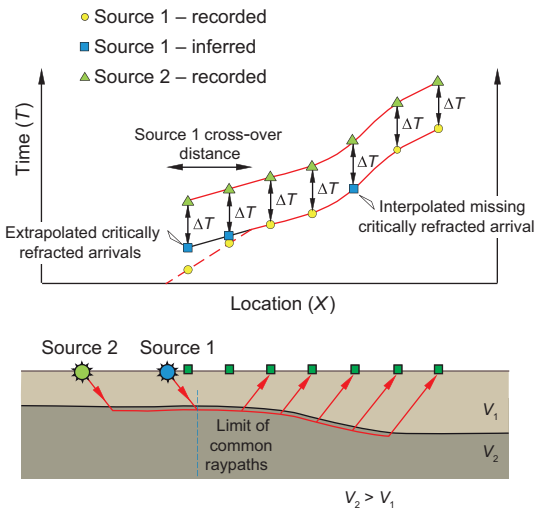

Figure A6.4 Phantoming of refracted arrivals. ΔT – average time difference between the two *T*–*X* graphs.

significant is that the refracted-arrival travel times from source 1 can be extrapolated to offsets less than the cross-over distance. If the right combination of source and detector locations has been used, it is possible to determine the travel times of refracted arrivals from any interface in both directions at every detector location. In this way the necessary information for modelling the data is obtained.

A6.3.3 Determining subsurface structure from travel times

There are several ways to determine subsurface structure from travel times, with a direct correlation between the resolution of the resulting cross-section and the effort required to produce it. We describe an inverse method known as the (*conventional*) *reciprocal method* (CRM), also known (mainly in Europe) as the *plus–minus method*. Central to CRM is a parameter known as *delay*.

A6.3.3.1 Delay

Delay is illustrated in Fig. A6.5, again using the simple case of a two-layer Earth, with a planar and horizontal velocity interface between the layers. As expected, the associated T–X graph comprises two straight branches. Arrival times for refracted arrivals at less than the cross-over distance would be determined using phantoming (see Section A6.3.2.4).

To understand delay, it is useful to recall that the travel time to any source–detector offset X can be defined in terms of a variable component, whose travel time is X/V_2, plus a constant component equal to the intercept time (see Eqs. (A6.3) and (A6.6)). As the topmost layer, having lower velocity (V_1), becomes thinner, the travel time curve shifts parallel to the time axis and the intercept time (T_{Int}) reduces, diminishing to zero when the topmost layer disappears (zero thickness) and the entire travel path is through the remaining single (originally higher) velocity layer. Referring to Fig. A6.5c, and comparing the raypaths for the cases when the upper layer is present and when it is absent, there are equivalent components of both travel paths where the ray travels within, and parallel to the top of, the layer whose velocity is V_2 (labelled A–B and E–F in the figure). Obviously, the difference in travel times is due to the sections of the travel paths that are different. This occurs near the source and near the detector, and the corresponding differences in travel times are known respectively as the *source delay* (δ_{source}) and *detector delay* (δ_{detector}).

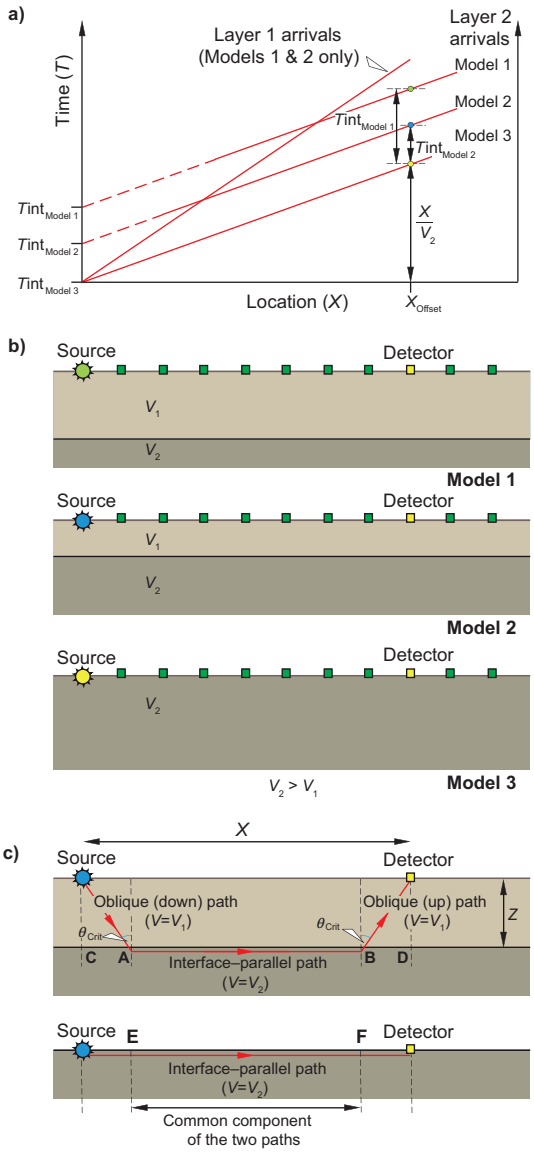

Figure A6.5 Relationship between depth to a horizontal refracting layer and T–X data. (a) T–X graphs for the three Earth models shown in (b); (b) velocity models comprising two layers separated by a horizontal interface, with the thickness of the upper layer varying; and (c) raypath when a near-surface lower-velocity layer is present and when absent.

The source and detector delays are due to the difference in travel times between oblique raypaths and the interface-parallel paths. The oblique paths (source–A and B–detector) are travelled at the lower velocity V_1 and the interface-parallel paths (source–E and F–detector) are travelled at the higher velocity V_2. For the case when there is no upper layer, the interface-parallel paths are equivalent to the distances C to A and B to D. In terms of the travel times of the oblique and parallel paths the two delays are:

$$\delta_{\text{source}} = T_{\text{source-A}} - T_{\text{CA}} = \frac{\text{source} - \text{A}}{V_1} - \frac{\text{CA}}{V_2} \quad \text{(A6.8)}$$

$$\delta_{\text{detector}} = T_{\text{B-detector}} - T_{\text{BD}} = \frac{\text{B} - \text{detector}}{V_1} - \frac{\text{BD}}{V_2} \quad \text{(A6.9)}$$

This definition of the delay, resulting from the difference in travel times between the oblique path between the ground surface and the refracting interface, and the interface-parallel component of this path is fundamental to delay-based inversion methods such as the CRM (see below).

From Fig. A6.5c, the travel times of both the interface-parallel and oblique paths can be stated in terms of the depth (Z) of the refractor and the critical angle (θ_{Crit}) as:

$$\delta_{\text{detector}} = T_{\text{B-detector}} - T_{\text{BD}} = \frac{Z}{V_1 \cos\theta_{\text{Crit}}} - \frac{Z \tan\theta_{\text{Crit}}}{V_2} \quad \text{(A6.10)}$$

Simplifying and rearranging Eq. (A6.10) gives:

$$Z = \delta_{\text{detector}} \frac{V_1}{\cos\theta_{\text{Crit}}} \quad \text{(A6.11)}$$

and expressed in terms of the velocities:

$$Z = \delta_{\text{detector}} \frac{V_1 V_2}{\sqrt{V_2^2 - V_1^2}} \quad \text{(A6.12)}$$

Note that these equations assume locally horizontal velocity layering, which is an acceptable approximation unless the structure of the subsurface is very complex (see Section A6.3.3.3).

Compare Eqs. (A6.11) and (A6.12) with Eqs. (A6.5) and (A6.7). For horizontal interfaces, the upward and downward components of the raypaths are identical and, therefore, so too are the source and detector delay times, which correspond with half the intercept time. It should be of no surprise that the equations are the same, except that half the intercept time is replaced by the delay time.

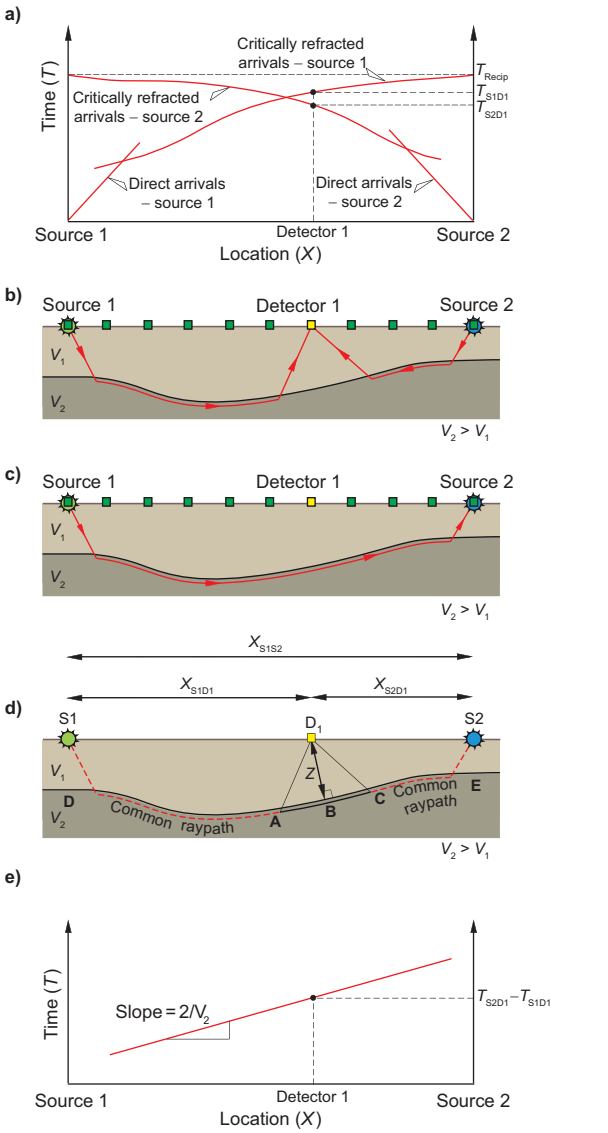

Figure A6.6 Schematic illustration of delay and the CRM. (a) T–X graphs; (b) refracted ray paths to the same detector (D1) from two sources located in opposite directions; (c) ray path associated with the reciprocal time (T_{Recip}); (d) the common oblique (A–D1 and C–D1) and interface-parallel (A–B–C) raypaths for determining delay; and (e) velocity function.

A6.3.3.2 Conventional reciprocal method

The principles of the CRM are illustrated in Fig. A6.6, which shows a T–X graph where the refracted arrivals are non-linear branches (Fig. A6.6a), indicative of an irregular refracting interface. Central to the method is the determination of a delay for refracted arrivals from each layer at each detector location and the conversion of that delay into a depth. Importantly, non-planar velocity interfaces can be mapped. Reversed data are required and the procedure is illustrated for arrivals at one of the detectors (D1). First the reciprocal time (T_{Recip}) must be determined, and as shown in Fig. A6.6c, this coincides with the raypath from either of the sources to a detector at the location of the other source. It is again useful to express the travel times in terms of a variable component plus the (constant) delay components associated with the upward and downward paths (see Eqs. (A6.3) and (A6.6)). It is also convenient to express the distance between the two sources (X_{S1S2}) as the sum of the distances from each source to the detector (X_{S1D1} and X_{S2D1}). Referring to Fig. A6.6d, and where δ_{source} and δ_{detector} are the source and detector delays, respectively,

the travel time between S1 and S2 (T_{S1S2}), i.e. the reciprocal time (T_{Recip}), is:

$$T_{S1S2} = T_{Recip} = \delta_{source1} + \delta_{source2} + \frac{X_{S1D1}}{V_2} + \frac{X_{S2D1}}{V_2} \quad \text{(A6.13)}$$

Consider now the travel times from each source to the detector (Fig. A6.6b) defined in the same way:

$$T_{S1D1} = \delta_{source1} + \frac{X_{S1D1}}{V_2} + \delta_{detector} \quad \text{(A6.14)}$$

$$T_{S2D1} = \delta_{source2} + \frac{X_{S2D2}}{V_2} + \delta_{detector} \quad \text{(A6.15)}$$

Note that the expressions for the travel times of the variable component of the travel time of the critically refracted arrivals are for offsets measured at the surface. For example, the distance D to E along the refractor is assumed to be equal to X_{S1S2} (Fig.A6.6d). This is acceptable when the refractor is sub-horizontal and sub-planar, but as the interface deviates from this ideal geometry the expression becomes increasingly inaccurate.

Adding Eqs. (A6.14) and (A6.15) (adding the raypaths in Fig. A6.6b) gives:

$$T_{S1D1} + T_{S2D1} = \delta_{source1} + \delta_{source2} + \frac{X_{S1D1}}{V_2} + \frac{X_{S2D1}}{V_2} + 2\delta_{detector} \quad \text{(A6.16)}$$

Subtracting Eq. (A6.13) (subtracting the raypath shown in Fig. A6.6c) gives:

$$T_{S1D1} + T_{S2D1} - T_{Recip} = 2\delta_{detector} \quad \text{(A6.17)}$$

Referring to Fig. A6.6d, the raypath intervals shown as broken lines are the intervals common to the raypaths in parts (b) and (c) of the figure. They have been cancelled by subtraction leaving two oblique paths (A–D1 and C–D1) from the two source-to-detector paths and an interface-parallel path (A–B–C) from the source-to-source (reciprocal-time) path. The travel times for the oblique paths less that for the interface-parallel path represents twice the value of the detector delay (Eq. (A6.17)). A delay can be calculated from the travel times to any detector for which there is a forward and a reversed refracted-arrival travel time. If these are not recorded directly, they can be determined by extending the relevant parts of the *T*–*X* curve using phantoming (see Section A6.3.2.4).

In order to convert the detector delay times to an interface depth using Eqs. (A6.11) and (A6.12), the velocities of the various layers must be known. The upper-layer velocity is obtained from the slope of the branches defined by the direct arrival data. It may be adequately represented as a constant-velocity layer, or lateral and/or vertical velocity variations may need to be accounted for (see Palmer, 1986). The velocities of the second layer can be determined simply by subtracting the travel time of critically refracted arrivals to a detector from one of the sources, from the travel time from the other source to the same detector. Both arrivals must be refracted arrivals from that layer. The resulting values define the *velocity function* which will comprise a line whose slope is $2/V_2$, where V_2 is the velocity of the layer in the region below the two detectors (Fig. A6.6e). If the layer velocity is constant, so too is the slope of the velocity function. Changes in slope are indicative of lateral changes in velocity, in which case a series of straight-line segments can be fitted to the data.

A6.3.3.3 Other interpretation methods

The conventional reciprocal method produces a reliable velocity cross-section in the majority of cases, but the method relies on some significant simplifying assumptions. Firstly, it assumes that first arrivals are either direct arrivals or refracted, which implies the subsurface comprises a series of layers between which the major changes in velocity occur. The most important assumption is illustrated in Fig. A6.7a, where the triangle A–detector–C is assumed to be an isosceles triangle, i.e. the refractor can be adequately represented as a straight line over the distance AC, and its velocity, and that of the overlying layers, is constant over this distance. The assumption is made when deriving both the delay time/interface depths (two delays are halved) and the velocity functions (two delays are assumed to cancel). Moreover, the base of the triangle is assumed to be horizontal, since the delay is converted to a depth vertically below the detector. The result is that subsurface features whose lateral extents are less than the distance AC tend to be averaged out, leading to an over-smoothed model of the subsurface structure. When there are significant velocity gradients within the layers or the structure of the interface is complex, the first arrivals may be diving waves or diffractions (Figs. A6.7b and f), invalidating the assumptions behind the CRM.

There are alternatives to the CRM which are designed to allow complex structure to be resolved. The *generalised reciprocal method* as described by Palmer (1986) is a development of the CRM which uses the travel times of refracted arrivals that leave the interface at a common location rather than those recorded by the same detector.

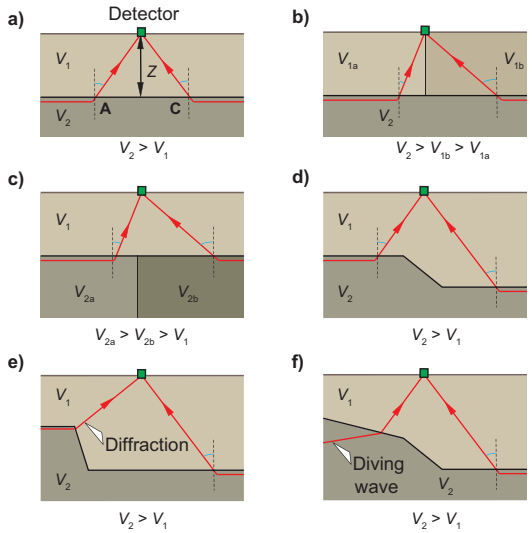

Figure A6.7 Velocity distributions affecting the validity of the CRM. A refracting layer with constant velocity which is planar between points A and C (a) is assumed by the CRM. Lateral variations in velocity (b and c), short-wavelength variations in refractor depth (d), and (e and f) the first arriving wave not a headwave: all invalidate the CRM.

Methods involving forward modelling of the paths of the seismic waves through a velocity cross-section of the subsurface are also available, and these may allow diffracted and diving wave arrivals to be modelled (e.g. Whiteley, 2004).

A third approach to modelling seismic refraction data is tomographic inversion (see Section 6.8.2). Modelling in this way can be comparatively fast, since it is not necessary to group arrivals manually according to travel paths. The subsurface velocity model produced is continuous and smooth because the data are matched entirely with curved ray paths, i.e. there are no discrete layers in the model. The effectiveness of the method is reduced by the non-ideal distribution of raypaths, because both source and receiver are above the target area, so the preferred wide range of directions is not achieved. A starting model is required for the inversion, which may be derived from one of the methods described above, and the result is often heavily dependent on the model chosen.

The relative merits of the different approaches to the interpretation of seismic refraction data are enthusiastically debated by their proponents: see for example Whiteley and Eccleston (2006) and Palmer (2010) and references therein. Like any geophysical inversion method, assumptions are made about the nature of the subsurface, and if those assumptions are valid the results are more reliable.

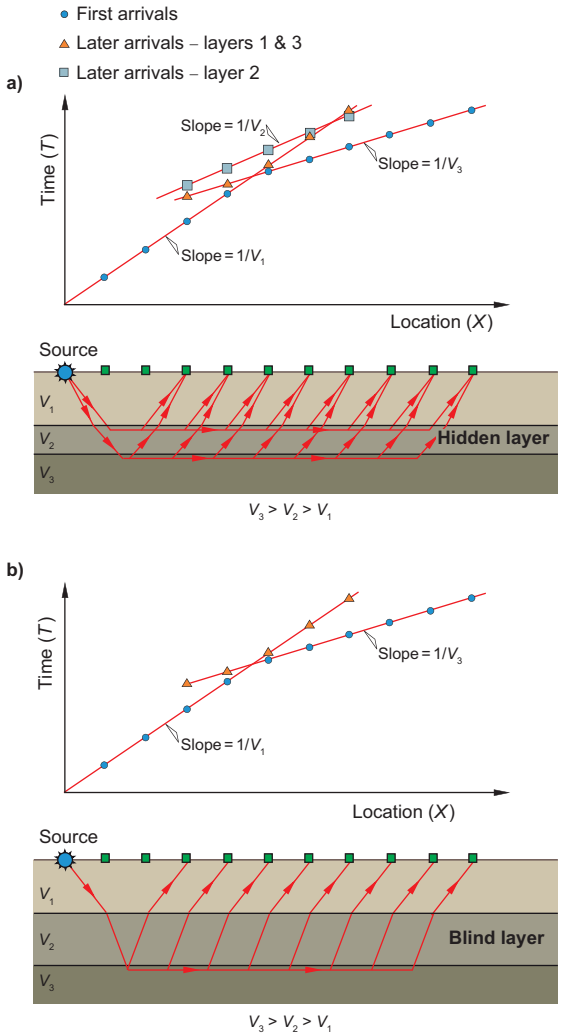

Figure A6.8 Hidden and blind seismic layers and their T–X graphs. (a) Thin 'hidden layer' (V_2), and (b) low-velocity 'blind layer' (V_2). Direct arrivals are not shown.

The choice of interpretation method depends on time available and what are considered to be likely subsurface conditions, e.g. continuously varying velocity versus a layered structure, and the degree of complexity.

A6.3.4 Interpretation pitfalls

The key to successful interpretation of seismic refraction data is sufficient source locations so that arrivals can be assigned to branches with confidence. There are, however, two situations where the analysis of first arrivals described previously will produce erroneous results.

Subsurface layers that are thin and/or have velocity (V_2) similar to the layer immediately above (V_1) may not give rise to first arrivals (Fig. A6.8a). These layers

are known as *hidden layers*. If the arrivals are of high amplitude, even though they are secondary, they may be recognised. More likely, the layer will be missed and the estimated depths, and possibly velocities (if the hidden layer changes thickness or velocity), of all the underlying velocity (V_3) structure will be incorrect. The erroneous interpretation replaces the hidden layer with a downward continuation of the overlying layer, which results in underestimation of the depths of features beneath the hidden layer.

Another problem arises when a layer has lower velocity than the layer immediately overlying it. In this case, critical refraction cannot occur at the top of the layer. The down-going seismic waves are refracted away from the interface and headwaves are not created (see Fig. 6.9b), so there are no refracted arrivals. The effect is known as a *velocity inversion*. On the *T*–*X* graph, what is, for example, a three-layer case produces only two branches etc. (Fig. A6.8b).

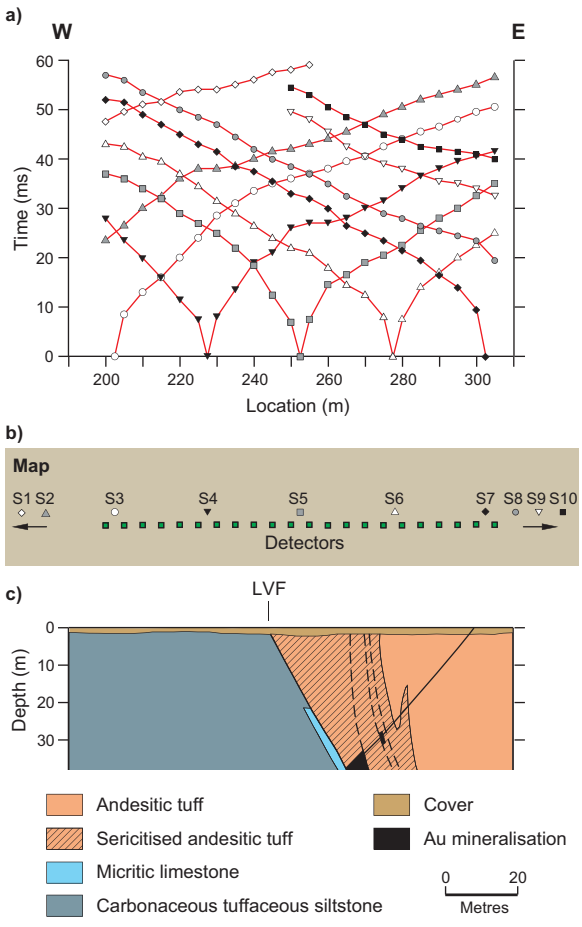

Figure A6.9 London-Victoria seismic refraction survey. (a) Travel time data, (b) geophone spread and shot locations (S1–10), and (c) geological cross-section along the line of the seismic survey based on Govett *et al.* (1984). LVF – London-Victoria Fault. Redrawn, with permission, from Whiteley (2004).

The underlying low velocity layer cannot be detected (with the seismic refraction method), so it is known as a *blind layer*. Blind layers cause erroneous interpretations of the underlying layers. The velocities will be correct if the

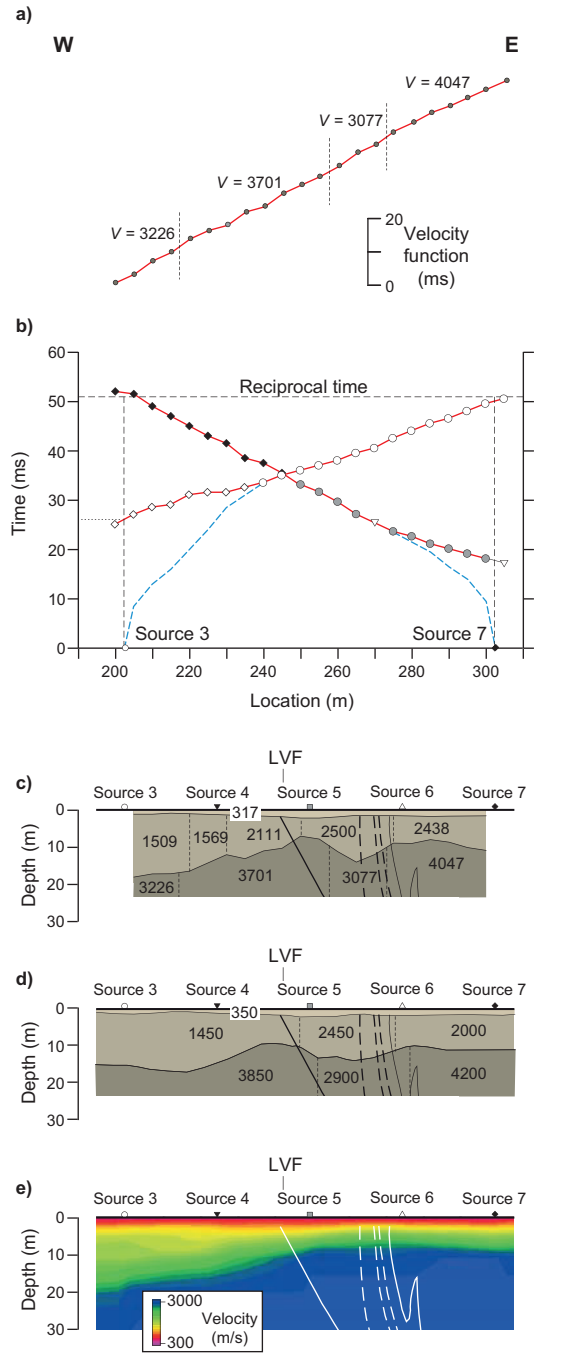

Figure A6.10 Interpretation results of the London-Victoria refraction dataset for various interpretation methods. (a) CRM velocity function for the deeper layer; (b) travel times for refracted arrivals from the deepest layer for sources S3 and S7; (c) CRM velocity model; (d) velocity model from ray-tracing of first arrivals, redrawn, with permission, from Whiteley (2004); and (e) tomographic inversion model. Geological contacts and faults superimposed from Fig. A6.9c. Velocities are in m/s. LVF – London-Victoria fault.

underlying layers have constant thickness, but the depths will be overestimated. As a general rule, velocity inversions are quite rare, but when they occur there is usually an anomalously high-velocity layer at shallow depth rather than a deeper layer with anomalously low velocity. Common examples are permafrost layers in polar regions, and caliche or laterite (see Fig. 6.37) horizons in arid climates. Velocity inversion due to a low-velocity layer may occur when there is a peat or coal horizon in the subsurface.

The presence of hidden layers and velocity inversions can be recognised from velocity information obtained from downhole velocity logs and by interpreting the refraction data in conjunction with other kinds of geological and geophysical data. Otherwise, they represent a fundamental limitation of the seismic refraction method.

A6.3.5 Example – mapping prospective stratigraphy using the CRM

This example of the interpretation of seismic refraction data uses a dataset recorded along a traverse across a mineralised zone of the London-Victoria gold deposit near Parkes, New South Wales, Australia (Whiteley, 2004). It is located within the area of the aeromagnetic data described in Section 3.11.4 (see Fig. 3.76). Mineralisation occurs in a brecciated and altered andesitic tuff adjacent to the steeply dipping London-Victoria fault (Govett *et al.*, 1984). Other lithologies in the vicinity are also tuffaceous. Bedding is nearly vertical and weathering reaches depths of up to 25 m. The local geology, survey layout and first-arrival travel time data are shown in Fig. A6.9. Geophones were laid out over a distance of 105 m with 10 shots recorded: five off-end (S1–2 and S8–10), two end (S3 and S7) and three within the spread itself (S4–5 and S6), with one of these being a centre shot (S5) (Fig. A6.9b). The detector spacing was 5 m and the shot spacing was 25 m. Three branches are evident in the *T*–*X* graph (Fig. A6.9a) and are indicative of three main velocity layers in the subsurface.

The CRM applied to the London-Victoria dataset is illustrated in Fig. A6.10a to c. Figure A6.10b shows the results of phantoming to create a single set of travel times across the whole survey area. In this case, the times of refracted arrivals from the deeper layer for sources S3 and S7 are shown. Figure A6.10a shows the velocity function and interpreted constant-slope segments for the same set of arrivals. The velocity cross-section is shown in Fig. A6.10c. The three layers are consistent with a geological section comprising unconsolidated cover overlying regolith, with fresh higher-velocity material at depth. The lateral changes in velocity in the subsurface layers are consistent with lithological variations in the steeply dipping succession. In particular, the lower-velocity zone in the lowest layer, between sources S5 and S6, coincides with the zone of alteration associated with the mineralisation.

Figure A6.10d shows the velocity cross-section model obtained from a ray-tracing method that accounts for diffracted first arrivals (Whiteley, 2004). The basic features of the CRM inversion are retained but the lateral positions of features are different. This occurs because some of the first arrivals are modelled as diffractions and not refractions, so an assumption inherent in the CRM is violated. Figure A6.10e shows the resultant velocity model from a tomographic inversion applied to the data shown in Fig. A6.9a. The results are broadly consistent with the CRM and ray-tracing models, and the matches to the observed data are equally good. However, the results are harder to relate to the geology and, importantly, the low-velocity region associated with the mineralised fault is not apparent.

Summary

- The seismic refraction method is used to map variations in seismic velocity in the subsurface. The method maps major velocity boundaries and provides accurate information about locations in the subsurface.
- Data are mostly 2D, i.e. recorded along traverses, and require less processing than seismic reflection data.
- Travel times of direct and headwave/diving-wave arrivals, usually just those arriving first at a detector, are plotted as a time–distance (*T*–*X*) graph.
- The interpretation of a *T*–*X* graph is based on the identification of 'branches', i.e. sections of data where the arrival times define an approximate straight line. The number of branches equals the number of velocity layers in the subsurface.

- Unambiguous assignment of data points to branches requires data recorded with sources at several locations relative to the geophone spread, and in particular at both ends of the spread.
- Time–distance (*T–X*) data are mostly interpreted using inverse methods, for example the conventional reciprocal method. Integral to the method is the parameter 'delay'.
- A limitation of the seismic refraction method is its inability to detect blind layers, i.e. layers whose seismic velocity is less than that of the layer above them.

Review questions

1. On what basis is the first arrival recognised within a seismic trace?
2. Explain why recordings from multiple shot locations can prevent ambiguity in the interpretation of travel time data.
3. Explain the use of reciprocal times, parallelism and phantoming in the analysis of refraction time-travel graphs.
4. What are hidden and blind layers, and how do they affect the interpretation of seismic refraction data?
5. What is a delay time, and why is it important when interpreting seismic refraction data?

FURTHER READING

Lankston, R.W., 1990. High-resolution refraction seismic data acquisition and interpretation. In Ward, S.H. (Ed.), *Geotechnical and Environmental Geophysics,* Volume 1: *Review and Tutorial.* Society of Exploration Geophysicists, Investigations in Geophysics 5, 45–73.

This tutorial paper is written in the context of engineering and environmental applications of the seismic refraction method, but of course the principles described have general applicability. It is highly recommended because of its clarity and scope and because of the case studies provided.

REFERENCES

Ackermann, H.D., Pankratz, L.W. and Dansereau, D., 1986. Resolution of ambiguities of seismic refraction travel time curves. *Geophysics*, 51, 223–235.

Dentith, M. C., Evans, B.J., Paish, K.F. and Trench, A., 1992. Mapping the regolith using seismic refraction and magnetic data: Results from the Southern Cross Greenstone Belt, Western Australia. *Exploration Geophysics*, 23, 97–104.

Goulty, N.R. and Brabham, P.J., 1984. Seismic refraction profiling in opencast coal exploration. *First Break*, 2(5), 26–34.

Govett, G.J.S., Dobos, V.J. and Smith, S., 1984. Exploration rock geochemistry for gold, Parkes, New South Wales, Australia. *Journal of Geochemical Exploration*, 21, 175–191.

Hatherly P.J., 1982. A computer method for determining seismic first arrival times. *Geophysics*, 47, 1431–1436.

Lankston, R.W., 1990. High-resolution refraction seismic data acquisition and interpretation. In Ward, S.H. (Ed.), *Geotechnical and Environmental Geophysics*, Volume 1. Society of Exploration Geophysicists, Investigations in Geophysics 5, 45–73.

Lawton, D.C. and Hochstein, M.P., 1993. Physical properties of titanomagnetite sands. *Geophysics*, 45, 394–402.

Miller, K.C., Harder, S.H., Adams, D.C. and O'Donnell, T., 1998. Integrating high-resolution refraction data into near-surface seismic reflection data processing and interpretation. *Geophysics*, 63, 1339–1347. doi: 10.1190/1.1444435

Pakiser, L.C. and Black, R.A., 1957. Exploring for ancient channels with the refraction seismograph. *Geophysics*, 22, 32–47.

Palmer, D., 1986. *Refraction Seismics. The Lateral Resolution of Structure and Seismic Velocity*. Geophysical Press.

Palmer, D., 2010. Is visual interactive ray trace an efficacious strategy for refraction inversion? *Exploration Geophysics*, 41, 260–267.

Whiteley, R.J., 2004. Shallow seismic refraction interpretation with visual interactive ray trace (VIRT) modelling. *Exploration Geophysics*, 35, 116–123.

Whiteley, R.J. and Eccleston, P.J., 2006. Comparison of shallow seismic refraction interpretation methods for regolith mapping. *Exploration Geophysics*, 37, 340–347.